Classical and Quantum Mechanical Studies of Crystalline Ammonium Nitrate

Dan C. Sorescu[†] and Donald L. Thompson*

Department of Chemistry, Oklahoma State University, Stillwater, Oklahoma 74078

Received: August 31, 2000; In Final Form: November 6, 2000

Plane-wave ab initio calculations based on density function theory and the pseudopotential method have been used to investigate the structural and electronic properties of phases V, IV, III and II of ammonium nitrate (AN) crystal. The optimizations of the crystal structures have been done with full relaxation of the atomic positions and lattice parameters under the experimentally determined crystal symmetries. The periodic nature of the crystals has been considered in calculations by employing periodic boundary conditions in all three directions. For phases V, IV and II the predicted crystal structures were found in good agreement with those determined experimentally by neutron diffraction data, but for phase III the differences between the experimental and calculated values are more significant. Band structure calculations indicate that AN is an insulator with a band gap in the range 3.18−3.57 eV corresponding to its different phases. The isotropic compression of phase IV has been studied using ab initio total energy calculations in the pressure range 0−600 GPa. It has been found that over this pressure range the crystal volume is compressed by 71% of the equilibrium volume. The increase in pressure determines significant changes of the band structure, large broadening of the electronic bands together with a decrease of the band gap by about 40%.We have developed a set of intra- and intermolecular classical potentials to describe phase V of AN. These potentials are composed by pairwise Lennard-Jones, hydrogen-bonding terms and Coulombic interactions. Crystal-packing calculations performed with these potentials accurately reproduce the main crystallographic features of this phase. These potentials were further tested in isothermal−isobaric molecular dynamics simulations at atmospheric pressure. It is found that increasing the temperature does not change the translational and rotational order of the molecules inside the crystal. The thermal expansion coefficients calculated for the model indicate anisotropic behavior with large expansions along the *a* and *b* axes and a very small one along the *c* axis.

I. Introduction

The interest in understanding the physical and thermal properties of ammonium nitrate (AN) has a long history and is motivated by the wide use of this material as fertilizer and blasting agent. However, more recently new avenues for practical applications of AN have been evidenced, particularly in the field of solid oxidizers for rocket propulsion.[1,2] The interest in AN as a solid oxidizer is determined by the fact that it is a cheap and safe energetic material. Moreover, unlike ammonium perchlorate, which is widely used in solid rocket propellants, AN produces less environmentally hazardous combustion products. At the same time, AN has several physical-chemical properties which limit its direct use in rocket motors. Among these, particle degradation and caking have been related to its high hygroscopicity and with a phase transition near room-temperature involving a large volume change. Consequently, there is a direct interest for a more fundamental understanding of the properties of AN in its different phases, with the practical goal of developing better ways of stabilizing these phases.

At normal pressures AN is known to exists in five phases in the temperature range from zero to the melting point (442 K) (see Table 1). The structures of the low-temperature phase V (see Figure 1a) has been determined by neutron diffraction in two different studies.[3,4] It is an ordered structure with orthorhombic symmetry (*Pccn* space group) and $Z = 8$ molecules per unit cell. The symmetry is close to tetragonal as the lattice constants *a* and *b* are almost equal. In this phase there are two types of NO_3^- ions slightly distorted while the NH_4^+ ions are symmetrically equivalent. There are strong hydrogen bonds in this phase with the shortest O···H contacts being between 1.916 and 1.987 Å.

Upon heating above 257 K, AN transforms to another ordered phase, called phase IV (see Figure 1b). The temperature stability range of this phase is 257−305 K,[5,6] but for the anhydrous crystals the stability range is extended to 257−323 K. The structure of phase IV has been characterized by several X-ray[5,6]

TABLE 1: Crystallographic Parameters of Different Phases of Ammonium Nitrate As Proposed in Different Experimental Studies

	phase				
	AN V	AN IV	AN III	AN II	AN I
temp range (K)	0−255	255−305	305−357	357−398	398−442
cryst ordering	ordered	ordered	disordered	disordered	disordered
space group	*Pccn*[a]	*Pmmn*[c,d]	*Pnma*[f]	*P*$\bar{4}$21*m*[e]	*Pm*$\bar{3}$*m*[h,i]
a (Å)	7.8850	5.7507	7.7184	5.7193	4.3655
b (Å)	7.9202	5.4356	5.8447	5.7193	4.3655
c (Å)	9.7953	4.9265	7.1624	4.9326	4.3655
Z	8	2	4	2	1
space group	*Pccn*[b]	*Pmmn*[d,e]	*Pnma*[d,g]		
a (Å)	7.9804	5.7574	7.6772		
b (Å)	8.0027	5.4394	5.8208		
c (Å)	9.8099	4.9298	7.1396		
Z	8	2	4		

[a] Reference 3. [b] Reference 4. [c] Reference 5. [d] Reference 6. [e] Reference 7. [f] Reference 8. [g] Reference 9. [h] Reference 10. [i] Reference 11.

[†] Current-mailing address: Department of Chemistry, University of Pittsburgh, Pittsburgh, PA 15260.

10.1021/jp0031449 CCC: $20.00
Published on Web 01/03/2001

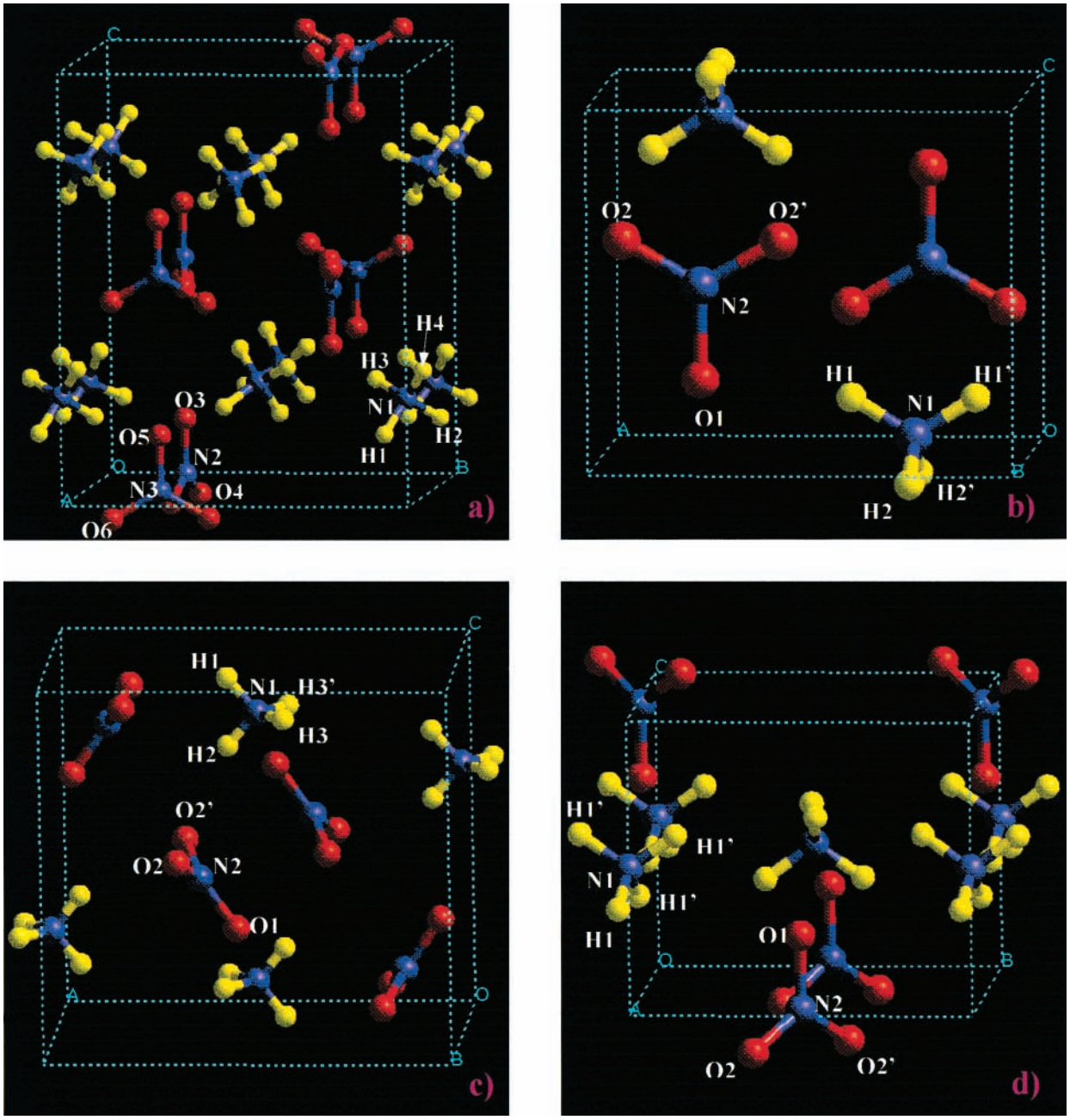

Figure 1. Crystal structure of AN in phases: (a) V; (b) IV; (c) III; (d) II.

and neutron diffraction studies.[7−9] The crystallographic parameters obtained in the latter studies[7−9] are summarized in Table 1. The structure is orthorhombic, with space group *Pmmn* with two NH_4NO_3 formula units per unit cell. A two-dimensional infinite network of hydrogen bonds between the N−H atomic pairs of the ammonium group and the O atoms of the nitrate exists in planes parallel to (001) with the adjacent molecular sheets connected by van der Waals forces.

At 305 K, AN undergoes a phase transition from the ordered phase IV to the disordered phase III by a dissolution−crystallization mechanism.[10] In the presence of small amounts of moisture (0.1 wt %) phase III is observed in the temperature range 305−357 K. The structure of phase III (see Figure 1c) has been determined by both X-ray[6] and neutron diffraction studies.[11] The crystal has an orthorhombic unit cell belonging to the *Pnma* space group with two equally populated orientations of the ammonium ion. As indicated by the shortest H···O distances (∼2.3 Å) the hydrogen bonds in this case are much weaker than in phase IV where the same short contacts have values of ∼2.0 Å. The weaker hydrogen bonding interactions in phase III allow the existence of large thermal vibrational motions of the ammonium ions leading to the disordered character for this phase.

On heating above 357 K phase III undergoes a phase transition to a tetragonal phase II (see Figure 1d).[12] This phase is stable in the temperature range 357−398 K, but for dry crystals the range of stability is 323 to 398 K. In the latter case phase III is not observed and a direct transition from phase IV to phase II takes place.[13] A neutron diffraction study[8] of phase II revealed that it has a tetragonal symmetry that is disordered and contains two equivalent alternative positions for each ammonium and nitrate ions. This phase transforms above 357 K in a disordered cubic phase (phase I)[14] which remains stable up to the melting point.

The transitions between different phases of AN have important consequences on practical applications. In particular, the

phase transition at 305 K is accompanied by a large change in volume (~3.84%) which causes irreversible growth, break up and caking of cast or pellitized AN. However, as the temperature stability of phase III is highly dependent on the amount of moisture, several doping and phase stabilizing agents have been considered. Among these, different transition metal oxides such as NiO[9,15] or CuO[16] have been shown to be quite effective in eliminating the IV → III phase transition, leading to a direct IV → II transition at 323 K. Other stabilization methods considered were based on the shift of the 305 K phase transition in a temperature range that is not affected by the external thermal conditions at which the material is used. For example, solid solutions of potassium nitrate (KN) and AN have been shown to lower the IV → III phase transition to temperatures below 273 K or even to eliminate this phase transition when the KN content is increased above 15%.[17]

The totality of experimental data indicate that the phase diagram of AN is extremely complex and a complete understanding of it is difficult to be achieved. However, the new applications of AN as a solid oxidizer for rocket propulsion require a precise control of the physical-chemical properties of this material and a detailed understanding at the atomic level of the interplay between the geometric, electronic and chemical properties. Quantum mechanical and classical molecular simulations can be used to answers such fundamental questions.

In the present study we make a first attempt to understand the complex nature of AN in its different phases. Particularly, the first objective of the work reported here is to investigate the structure and the electronic properties of AN crystal in different phases using first-principles calculations. For this purpose we use ab initio calculations based on density functional theory (DFT) and the pseudopotential method. The periodic nature of the crystal is considered in the present calculations by using boundary conditions in all three directions. The equilibrium structure of the crystal is obtained by full relaxation of the unit cell parameters allowed by the crystal symmetries as well as of the ionic positions inside the unit cell.

For energetic materials understanding of the combustion and detonation processes represents another important task, their mechanisms being not well-known. For example, it has been suggested that initiation of these processes in solid energetic materials is associated with the presence of "hot spots"[18] or regions of high shear stress[19] determined by a high density of dislocations. However, Gilman has questioned this interpretation and has emphasized the role played by excited electronic states in initiation of these processes.[20] In particular he has suggested that shock initiation can be determined by metallization of the solid as a result of highly compressed materials. Given the importance of the role played by compression effects on the electronic structure of solids we analyze such effects in the present study for phase IV of AN using ab initio calculations.

Ideally the equilibrium and dynamical properties of molecular crystals should be obtainable by the use of first-principles molecular dynamics simulations. Such calculations represent the state of the art but they are computationally extremely demanding. The alternative to this approach is to develop reliable intermolecular potentials to be used in classical molecular dynamics (MD) or Monte Carlo (MC) simulations. We have successfully developed such intermolecular potentials for a series of 30 nitramine crystals[21a−c] including some of the most important explosives such as hexahydro-1,3,5-trinitro-1,3,5-*s*-triazine (RDX), 1,3,5,7-tetranitro-1,3,5,7-tetraazacyclooctane (HMX) and 2,4,6,8,10-hexanitrohexaazaisowurtzitane (HNIW), and have analyzed the transferability of such potentials to a set of 50 other nonnitramine compounds.[21e] More recently we have also reported the development of a classical intermolecular potentials for the ionic molecular crystal ammonium dinitramide (ADN).[22]

In the present work we extend these studies and develop a set of intra- and intermolecular potentials to describe the structural properties of crystalline phase V of AN. These potentials will allow direct theoretical investigations of the response of AN crystal to different external stimuli such as heating or compression. In addition, such a potential model can be also used in theoretical crystal engineering to design crystals with different types of ionic packing.

The methodology followed to develop the AN intermolecular potential is similar to that we used previously for RDX,[21a] ADN[22] and NTO (5-nitro-2,4-dihydro-3*H*-1,2,4-triazol-3-one) crystals.[23] The intermolecular interactions are assumed to be describable by simple isotropic potentials such as the (6-exp) Buckingham potentials or the (6-12) Lennard-Jones potentials with explicit consideration of the electrostatic interactions between the charges associated with various atoms of different molecules. We find that for AN the crystalline structure can be reasonably predicted by using a superposition of Coulombic terms, 6-12 Lennard-Jones potentials, and 10-12 potentials to describe the hydrogen bonding. The Coulombic terms were determined by fitting partial charges centered on each atom of the NH_4^+ and NO_3^- ions to a quantum mechanically derived electrostatic potential. The parametrization of the potential function is done such that the model reproduces in molecular packing (MP) calculations the experimental structure of the crystal. The intramolecular part of the potential was parametrized based on the set of vibrational frequencies determined for NH_4^+ and NO_3^- ions by ab initio molecular orbital calculations. The total potential determined in MP studies was further tested in isothermal−isobaric molecular dynamics simulations (NPT-MD) over the range 4.2−250 K at atmospheric pressure.

The organization of the paper is as follows: In section II we describe the computational methods. In section III we present the results of total energy calculations for different phases of AN. In the case of AN IV phase we report also the results of hydrostatic compression up to 600 GPa. Section IV contains the results of lattice energy minimization by molecular packing calculations and the results of trajectories calculations in the constant temperature and pressure ensemble. Finally, we summarize the main conclusions in section V.

II. Computational Method

A. Total Energy Calculations. The calculations performed in this study were done using the commercial version of the software package CASTEP (Cambridge Serial Total Energy Package).[24] This program evaluates the total energy of periodically repeating geometries based on density-functional theory and the pseudopotential approximation. In this case only the valence electrons are represented explicitly in the calculations, the valence-core interaction being described by nonlocal pseudopotentials. Periodic boundary conditions are used, with the occupied electronic orbitals expanded in a plane-wave basis. The expansion includes all plane waves of kinetic energy, $\hbar^2k^2/2m < E_{cut}$ where k is the wave vector, m the electronic mass, and E_{cut} is the cutoff energy chosen to be 1200 eV. A gradient-corrected form of the exchange correlation functional (GGA) was used in the manner suggested by White and Bird.[25] The Brillouin zone was sampled with the Monkhorst−Pack scheme.[26]

The pseudopotentials used in this study are norm-conserving of the form suggested by Kleinman and Bylander,[27] and

optimized using the scheme of Lin et al.[28] The self-consistent ground state of the system was determined using a band-by-band conjugate gradient technique to minimize the total energy of the system with respect to the plane-wave coefficients. The optimization of different atomic configurations reported in this study was done using the Broyden−Fletcher−Goldfarb−Shanno (BFGS) minimization technique, with the following thresholds for the converged structure: energy change per atom less than 1.0×10^{-6} eV, residual force less than 0.02 eV/Å, the displacement of atoms during the geometry optimization less than 0.001 Å and the residual bulk stress less than 0.1 GPa. Pulay stress corrections were evaluated numerically based on the method introduced by Francis and Payne[29] using the total energy calculated at three different values of the kinetic energy cutoff. Besides optimizations of different phases at ambient pressures, in the case of phase IV we have done calculations at different pressures in the range 0−600 GPa.

B. Molecular Packing Calculations. A general procedure for testing empirical or semiempirical intermolecular potential energy functions for organic crystals is the use of molecular packing calculations.[30] The basic idea consists of minimization of the lattice energy with respect to the structural degrees of freedom of the crystal. For a crystal with Z molecules per unit cell (N atoms per molecule) at arbitrary positions, these degrees of freedom are determined by the $3NZ$ positions of the atoms in the unit cell as well as the dimensions and angles of the unit cell. This maximal number is decreased by symmetry imposed constraints on either lattice parameters or on different subsets of atomic coordinates when the atoms occupy special positions.

Significant reduction of the computational time necessary to minimize the lattice energy starting with a trial configuration can be obtained by performing symmetry-adapted energy minimizations. In the present study we have used for such calculations the general utility lattice program (GULP)[31,32] which is suitable for the treatment of both inorganic and organic systems with fully flexible molecules. Besides the minimization of the lattice energy this program has the capability of empirically optimizing potential parameters through a least-squares fitting procedure. Ideally, the fitting procedure should include not only the geometrical structure of the crystal of interest but also information related to the second derivative of the potential such as the elastic constants. However, in our case no such data related to the elastic stiffness tensor were available and consequently our fitting procedure was restricted to the geometrical parameters of the crystal.

The potential function used to describe the intermolecular interactions in crystalline AN was constructed as a sum of pairwise additive Lennard-Jones (LJ), hydrogen bonding (HB) and Coulombic (C) potentials of the form:

$$V_{\alpha\beta}^{\mathrm{LJ}}(r) = \frac{\mathrm{A}_{\alpha\beta}}{r_{\alpha\beta}^{12}} - \frac{B_{\alpha\beta}}{r_{\alpha\beta}^{6}} \tag{1}$$

$$V_{\alpha\beta}^{\mathrm{HB}}(r) = \frac{A_{\alpha\beta}^{\mathrm{H}}}{r_{\alpha\beta}^{12}} - \frac{B_{\alpha\beta}^{\mathrm{H}}}{r_{\alpha\beta}^{10}} \tag{2}$$

and

$$V_{\alpha\beta}^{\mathrm{C}}(r) = \frac{q_\alpha q_\beta}{4\pi\epsilon_0 r_{\alpha\beta}} \tag{3}$$

where $r_{\alpha\beta}$ is the interatomic distance between the atoms α and β belonging to different molecules, q_α and q_β are the corresponding electrostatic charges on these atoms, and ϵ_0 is the dielectric permittivity constant for vacuum.

The intramolecular interaction potential has been taken to be of the form

$$V_{\mathrm{intra}} = V_{\mathrm{stretch}} + V_{\mathrm{bend}} + V_{\mathrm{torsion}} \tag{4}$$

to describe the bond stretching, angle bending and torsional motion (only for the case of NO_3^-) of the isolated ions. The bond stretches are represented by harmonic potentials,

$$V_{\mathrm{stretch}} = \frac{1}{2}k_{\mathrm{ri}}(r_{\mathrm{i}} - r_{\mathrm{i}}^{0})^2 \tag{5}$$

where r_{i} are the intramolecular bond distances, k_{i} are the force constants and r_{i}^0 are the equilibrium bond lengths.

The bending potentials are represented by harmonic functions

$$V_{\mathrm{bend}} = \frac{1}{2}k_{\theta\mathrm{i}}(\theta_{\mathrm{i}} - \theta_{\mathrm{i}}^{0})^2 \tag{6}$$

where k_θ is the force constant and θ^0 the equilibrium value of the angle.

The torsional potentials are used only for the O−N−O−O atoms of the NO_3^- ions, which at equilibrium are in a plane. These potentials have the form

$$V_{\mathrm{torsion}} = 2k_\Phi \sin^2 \Phi \tag{7}$$

where k_θ is the force constant and Φ is the torsional angle.

Based on eqs 1−7 the lattice energy can be evaluated as the sum of intra- and intermolecular interactions between the ions in the central unit and all the other ions in the image cells. The evaluation of the Coulombic sums over the infinite periodic lattice has been done using the standard Ewald transformation technique[33] to improve the slow rate of convergence of these sums. Further details of the summations procedures of different energy terms over the lattice as well as of the adjustable parameter which determines the relative contribution of the direct and reciprocal-space terms in Ewald sum are given in ref 32.

The values of the force constants used in the intramolecular part of the potential were parametrized based on the ab initio calculated vibrational frequencies of the isolated NH_4 and NO_3 ions. These calculations have been done at MP2/6-31G** level[34] using Gaussian 98 program.[35] The values of harmonic vibrational frequencies determined at this level have been uniformly scaled by a factor of 0.9370.[36]

For the type of molecular ionic crystals described in this paper the most sensitive part of the intermolecular potential is the set of electrostatic point charges attributed to different atoms, the remaining intermolecular potential parameters depending highly on this set. However, the assignment of the electrostatic charges poses a problem in that the atom-centered monopole charge is not an observable quantity and cannot be obtained directly from either experiment or first principles calculations. There are several schemes for evaluating charges by empirical partition or by using a quantum mechanically derived wave function.[37] We have chosen to make the assignments for the atom-centered monopole charges by using the set that best reproduces the quantum-mechanically derived electrostatic potential that is calculated over grid points surrounding the van der Waals surface of the NH_4 and NO_3 ions. This method of fitting to the electrostatic potential was proposed by Breneman and Wiberg[38] and is incorporated in the Gaussian 98 package of programs[35] under the keyword CHELPG. We have used this method in

TABLE 2: Comparison of the Calculated and Experimental Crystallographic Lattice Parameters and of the Intra- and Intermolecular Geometrical Parameters for Phases V, IV, III, and II of AN

	lattice parameters		bond lengths			bond angles			hydrogen bonds parameters (calc over exp)		
phase	calc (Å)	exp (Å)		calc (Å)	exp (Å)		calc (deg)	exp (deg)		H···O (Å)	N−H···O (deg)
AN V[a]	*a*: 8.0750	7.8850[a]	N2−O1	1.2768	1.2639	O1−N2−O2	118.8	116.9	N1−H3···O1	1.844	172.2
	b: 8.0629	7.9202	N2−O2	1.2449	1.2234	O2−N2−O2′	122.3	126.3		1.889	168.0
	c: 9.9997	9.7953	N3−O3	1.2741	1.2658	O3−N3−O4	118.9	119.5	N1−H4···O2	1.921	168.0
			N3−O4	1.2463	1.2614	O4−N3−O4′	122.1	120.9		1.950	157.6
			N1−H1	1.0331	1.0629	H1−N1−H2	110.1	107.1	N1−H2···O3	1.905	172.1
			N1−H2	1.0403	1.0839	H1−N1−H3	109.5	107.8		1.836	170.0
			N1−H3	1.0421	1.0048	H1−N1−H4	109.6	109.2	N1−H1···O4	1.892	171.1
			N1−H4	1.0314	1.0198	H2−N1−H3	109.0	108.9		1.876	170.0
						H2−N1−H4	108.8	111.2			
						H3−N1−H4	109.8	112.4			
AN V[b]	*a*: 8.0598	7.9804[b]	N2−O1	1.2745	1.230	O1−N2−O2	119.0	119.5	N1−H3···O1	1.890	173.0
	b: 8.0662	8.0027	N2−O2	1.2459	1.232	O2−N2−O2′	122.0	121.1		1.958	168.4[f]
	c: 10.0276	9.8099	N3−O3	1.2783	1.203	O3−N3−O4	118.8	117.3	N1−H4···O2	1.830	172.6
			N3−O4	1.2445	1.234	O4−N3−O4′	122.4	125.3		1.916	167.1
			N1−H1	1.0328	1.000	H1−N1−H2	109.8	110.5	N1−H2···O3	1.969	166.8
			N1−H2	1.0304	1.002	H1−N1−H3	110.0	110.1		1.939	164.7
			N1−H3	1.0409	0.986	H1−N1−H4	109.5	105.2	N1−H1···O4	1.911	170.7
			N1−H4	1.0428	1.022	H2−N1−H3	108.7	108.5		1.987	170.7
						H2−N1−H4	109.7	111.2			
						H3−N1−H4	109.2	111.3			
AN IV	*a*: 5.8008	5.7507[c]	N2−O1	1.2882	1.274	O1−N2−O2	118.9	120.0	N1−H1···O1	2.057	151.9
	b: 5.4072	5.4356	N2−O2	1.2425	1.254	O2−N2−O2′	122.1	120.0		2.050	154.4
	c: 5.0362	4.9265	N1−H1	1.0352	1.069	H1−N1−H1′	111.4	115.7	N1−H2···O1	2.107	171.9
			N1−H2	1.0296	1.072	H1−N1−H2	109.2	107.9		2.161	172.6
						H2−N1−H2′	108.5	109.4	N1−H1···O2	2.319	148.7
										2.326	147.9
AN III	*a*: 8.4142	7.7184[d]	N2−O1	1.2696	1.231	O1−N1−O2	119.5	119.7	N1−H2···O1	1.921	153.1
	b: 5.8052	5.8447	N2−O2	1.2513	1.275	O2−N1−O2′	120.9	120.7		2.330	138.5
	c: 7.1671	7.1624	N1−H1	1.0267	1.022	H1−N2−H2	109.7	101.1	N1−H3···O1	2.081	153.8
			N1−H2	1.0303	1.041	H1−N2−H3	108.1	114.9		2.299	139.1
			N1−H3	1.0336	1.174	H2−N2−H3	109.8	114.1	N1−H1′···O2	2.326	138.1
										2.395	147.0
									N1−H3′···O2	2.081	153.8
										2.236	152.5
AN II	*a*: 5.7808	5.7193[e]	N2−O1	1.2366	1.239	O1−N2−O2	120.0	120.8	N1−H1···O1	2.705	102.9
	c: 4.8355	4.9326	N2−O2	1.2652	1.212	O2−N2−O2′	119.9	118.4		2.658	105.2
			N1−H1	1.0352	0.988	H1−N1−H1′	109.5	109.5	N1−H1···O2	1.880	169.5
										2.008	163.3

[a] Reference 3. [b] References 4. [c] References 5 and 6. [d] Reference 8. [e] Reference 7. [f] The original value of 147.4° is erroneous and should be corrected to 168.4°.

conjunction with Møller−Plesset perturbation theory at the MP2/6-31G** level.

The remaining intermolecular potential parameters were fitted using the GULP program to reproduce the experimental observed structure. The starting set of Lennard-Jones and hydrogen bonding parameters used in the fitting procedure was taken to be identical to that we have previously developed for ammonium dinitramide (ADN) crystal.[22] On the basis of systematic molecular packing calculations we have ascertained that a reasonable agreement with the experimental crystallographic structures for phase V of AN can be achieved by transferring the H···H, N···N, O···O and N···H interaction potentials from the ADN crystal model[22] and refitting the N···O and H···O intermolecular potentials. The full list of potential parameters determined from these calculations is presented in section III.

C. Constant Pressure and Temperature Molecular Dynamics Calculations. Additional tests of the intra- and intermolecular potentials for phase V of AN have been done by constant pressure and temperature (NPT) molecular dynamics simulations. This method yields average equilibrium properties of the lattice as functions of temperature and pressure.

We have used the Nosé−Hoover barostat algorithm[39] as implemented in the program DL_POLY_2.0,[40] to simulate the AN crystal at various temperatures in the range 4.2−250 K and at atmospheric pressure. The equations of motion for both the ions and the simulation cell are integrated using the Verlet leapfrog scheme.[41]

The MD cell consists of boxes of $3 \times 3 \times 3$ crystallographic unit cells. This choice of this simulation box allows the use of a cutoff distances for the intermolecular potentials of about 9.5 Å The initial configuration corresponding to the lowest temperature was chosen to be identical to that for the experimental structure. The system was then equilibrated at that temperature and atmospheric pressure. In all production runs done using Nosé−Hoover implementation for the NPT ensemble the system was integrated for 28000 time steps (1 time step $= 0.75 \times 10^{-15}$ s), of which 4000 steps were equilibration. In the equilibration period the velocities were scaled after every 5 steps so that the internal temperature of the crystal mimicked the imposed external temperature. Then, average properties were calculated over the next 24000 integration steps ($\Delta t = 18$ ps) in the simulation. In subsequent runs, performed at successively higher temperatures the initial configurations of the molecular positions and velocities were taken from the previous simulation at the end of the production run.

The lattice sums were calculated subject to the use of minimum-image periodic boundary conditions in all dimensions.[41] The interactions were determined between the sites (atoms) in the simulation box and the nearest-image sites within

the cutoff distance. In these calculations, the Coulombic long-range interaction were handled using Ewald's method.[41]

The main quantities obtained from these simulations were the average lattice dimensions and the corresponding volume of the unit cell. Additional information about the structure of the crystal has been obtained by calculating the radial distribution functions (RDF) between different atomic sites. Such quantities have been calculated from recordings done at every 10th step during trajectory integrations.

III. Results and Discussion

A. Ab Initio Total Energy Calculations. *A1. Geometric and Electronic Properties of AN Phases.* The first investigations we considered in this study were related to prediction of the bulk structure of AN in crystallographic phases V, IV, III and II based on ab initio total energy calculations. For this purpose we performed geometry optimizations of both the unit cell parameters and of the ionic positions under the experimentally determined space group symmetries (see Table 1). The relaxation of the unit cell was done with respect to the independent lattice parameters, for example *a*, *b*, and *c* lattice parameters of AN V but only a and c for AN II while the lattice angles were fixed at 90.0°. In these calculations the sampling k-points were generated using the Monkhorst−Pack scheme[26] with mesh parameters 2 × 2 × 2 for AN V, 2 × 3 × 3 for AN IV, 2 × 3 × 2 for AN III and 4 × 4 × 4 for AN II along the three reciprocal lattice vectors. The results of these calculations are given in Table 2.

The analysis of results given in Table 2 shows that the agreement between the calculated and the experimental crystallographic lattice parameters is good for the case of AN V, AN IV and AN II phases with maximum deviations from the experimental data of 2.4%[3] (or 2.2%[4]) for phase V, 2.16%[7] for phase IV and 1.96%[8] for phase II, respectively. In the case of the phase III the calculated parameters, particularly lattice dimension *a*, differ more significantly from the measured values.[11] These differences might be due to different dynamical contributions such as the orientational disorder of ammonium ions and the temperature effects which are not considered in our ab initio calculations. However, we find that in the case of phase II which possess dynamical disorder of the ammonium ions, this affects less significantly the lattice parameters and correspondingly the agreement between the experimental and the predicted values is much better than in the case of AN III phase.

In the case of phase V of AN we have considered both structures proposed in neutron powder diffraction studies, herewith called V(1)[3] and V(2).[4] These two studies indicate essentially the same features for the phase V but some differences are also present. In particular, the *b* axis of the unit cell for V(2) is equivalent to the −*b* axis for V(1). Additional differences appear for some geometrical parameters of the H atoms, particularly the H···O distances as well as for the lengths of N−O bonds that differ by up to 0.03 Å in some instances. As can be seen in Table 2 both sets of calculations for phase V indicate a distortion of nitrate group from the ideal 3-fold-symmetric structure with an elongated N2−O1 bond length and an enlarged bond angle O2−N2−O2′. This distortion is also seen in the experimental structure proposed by Choi and Prask[3] but not in that found by Ahtee et al.[4] As indicated by the short N−H···O distances, all hydrogen atoms of the ammonium ions are involved in strong hydrogen bonding. Our calculations predict geometrical parameters for the hydrogen bonding in very good agreement with data reported by Choi and Prask.[3] For the

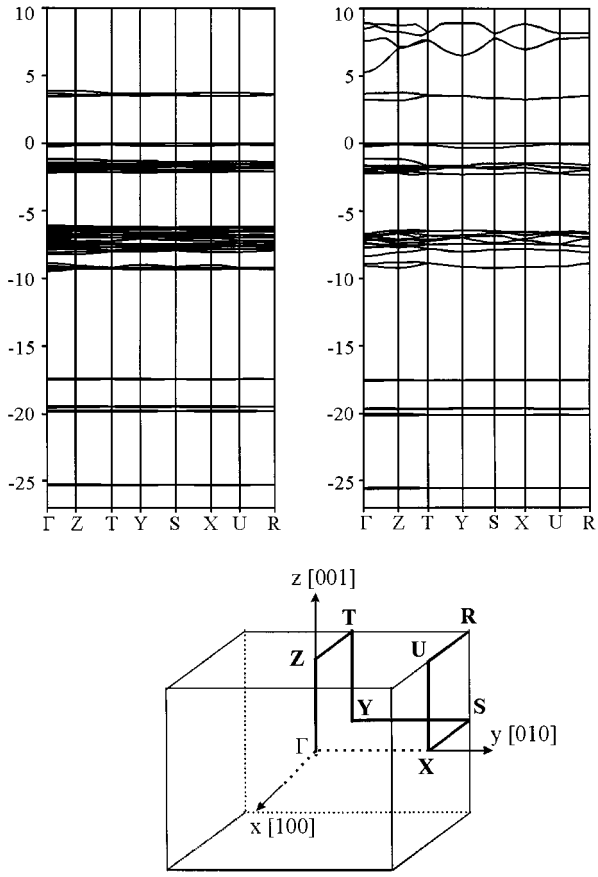

Figure 2. Band structures for phases V (a) and IV (b) of AN along different symmetry directions along the Brillouin zone. The energies of the highest occupied crystalline orbitals has been set to zero.

V(2) symmetry configuration our calculations give shorter N−H···O distances than found experimentally by Athee et al.,[4] in agreement with the V(1) proposed structure.[3] A possible explanation for the differences observed experimentally for the V(1) and V(2) structures can be due to the different temperatures at which the measurements have been done, i.e., 78 K for V(1) and 233 K for V(2). In the case of V(2), the increased external temperature influences more significantly the positions and amplitudes of motions for H atoms and consequently affects more significantly the N−H···O bonding parameters.

A similar good description is found in Table 2 for the phase IV of AN. Our calculations confirm that the N−O1 bond length is longer than N−O2 as seen experimentally. This is also in line with the fact that O1 atoms are involved in strong hydrogen bonds and consequently shorter N−H1···O1 and N−H2···O1 distances, while the O2 atoms are not. In this latter case the H1···O2 intermolecular distance is about 2.32 Å, almost at the upper limit of 2.4 Å considered for hydrogen bonding to oxygen.[42] The superposition of these types of interactions determines the existence of infinite hydrogen-bonded chains parallel to the *a* axis and formed by N1−H1···O1···H1−N1 bonds, with a layered structure parallel to (001). The weaker interactions H1···O2 causes the existence of a cleavage plane parallel to the (001) plane.

For the AN II phase the overall agreement between the predicted and experimental results is surprisingly good when we consider that this phase is disordered and exists only at elevated temperatures, above 357 K. This indicates that phase II is characterized by a dynamic type of disorder of the NH_4 ions which, when mediated over different configurations, has a relatively small effect on the tetragonal crystal symmetry.

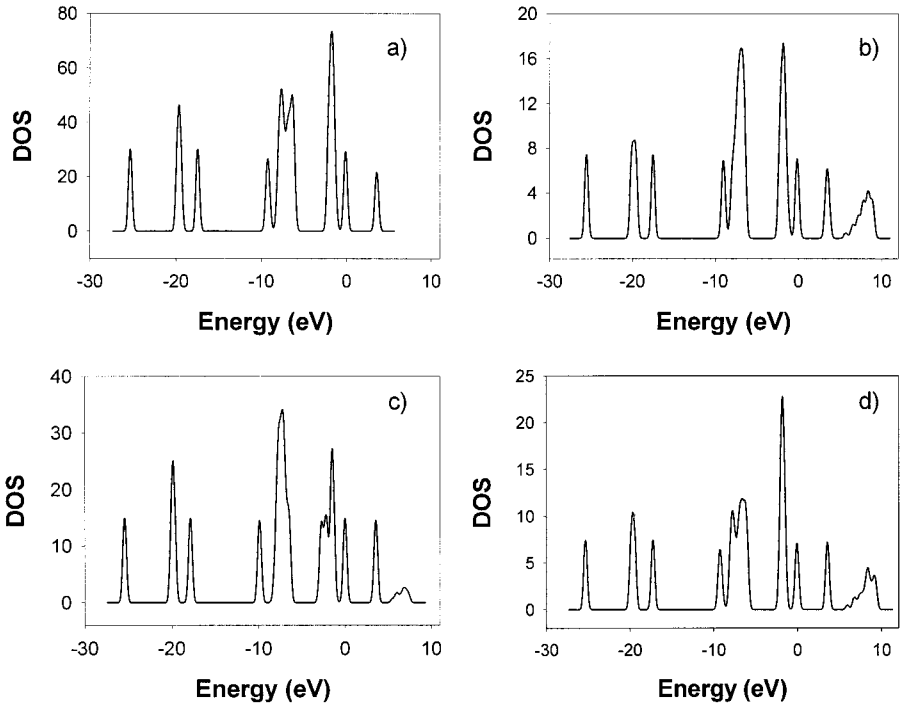

Figure 3. Calculated total density of states (DOS) of AN in phases V (a), IV (b) III (c), and II (d). The energies of the highest occupied crystalline orbitals have been set to zero.

We have calculated the self-consistent band structure along different symmetry directions for the optimized structures of AN in its different phases. The results are shown in Figure 2 and the corresponding total densities of states are given in Figure 3. In both Figures 2 and 3 the energy of the highest occupied crystalline orbital has been set to zero. As can be seen AN in the different phases is an electrical insulator. The bands are almost flat along the Brillouin zone consistent with the ionic character of the crystal. Moreover, different groups of occupied bands are well separated by the neighboring bands by distances of up to few eV. From these calculations we determined the band gaps at the Γ point to be equal to 3.44 eV for AN V, 3.37 eV for AN IV, 3.46 eV for AN III and 3.51 for AN II phases, respectively. However, for phases IV and III the minimum of the band gap takes place at points different from the Γ point, namely at the *Z* point for AN IV (gap = 3.18 eV) and along the *G*−*Z* direction for AN III case with a minimum gap of 3.37 eV.

A better understanding of the character of these bands can be obtained by projecting the calculated charge density on the atom-centered orbitals. These representations, also called projected density of states (PDOS), are given in Figure 4 for the case of individual atoms in NH_4 and NO_3 ions corresponding to phase AN IV. As can be seen, the individual s and p bands corresponding to different atoms can be identified clearly in the total DOS spectrum excepting the regions between (−10, −5) eV and (−2, −1) eV where a mixing of states from both the ammonium and nitrate ions is present, consistent with the molecular character of the crystal. Comparing the results in Figure 4a,d shows that the top of the valence band is represented by the O(2p) levels. The next occupied band centered around −2 eV has contributions from both O(2p) and N1(2p) of the ammonium ions. The bottom of the conduction band or the lowest unoccupied crystalline orbitals between 3.5 and 4.5 eV are formed by contributions from both O(2p) and N2(2p) of the nitrate ions. These bands are separated by about 2 eV from the next, more diffuse bands with contributions from both ammonium and nitrate ions.

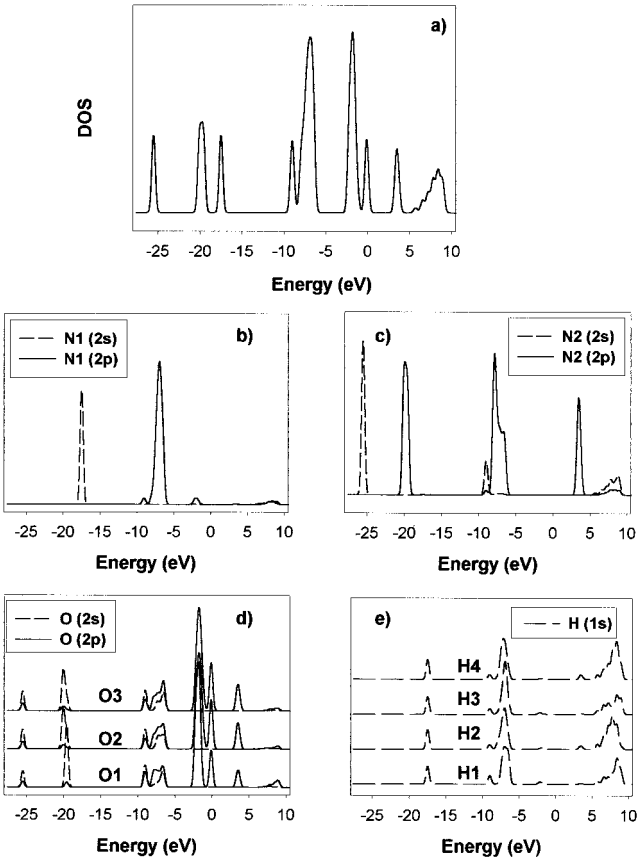

Figure 4. Projected density of states (PDOS) on the individual atoms of NH_4 and NO_3 ions corresponding to phase AN IV.

Additional insight in the ionic character of the NO_3 and NH_4 groups can be obtained by investigating the electronic charges distributions. We present in Figures 5 and 6a contour plots of charges for the case of phases V and IV. In the first case we indicate the charge distributions through planes along [110]

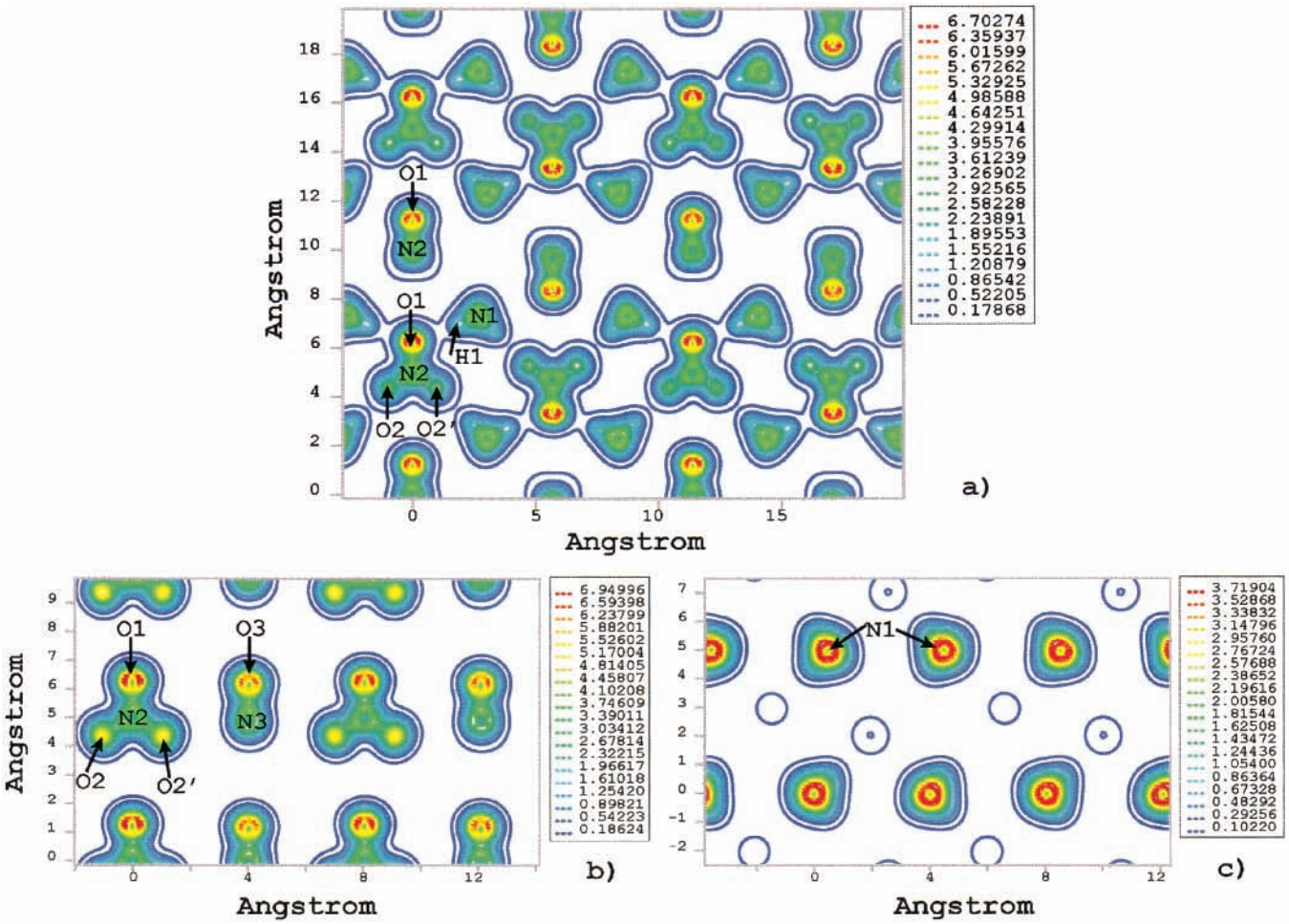

Figure 5. Contour plots of the valence electron density (units of electrons/Å^3) in the case of phase AN V. The contours are taken (a) along the [110] plane which bisects along the first diagonal the aOb plane, (b) parallel to (100) plane passing through NO_3 groups, and (c) parallel to (100) plane, passing through NH_4 ions.

direction (Figure 5a), parallel to the *aOc* planes passing through the planar NO_3 ions (Figure 5b), and through NH_4 ions (Figure 5c). In Figure 6a, the charge section was taken also in a plane parallel to *aOc* face which passes through the N atom of the nitrate and ammonium groups. As can be seen in both cases the valence charge density is highly concentrated around individual N and O sites of NO_3^- and N atoms of NH_4^+ in accordance with the anionic and cationic character of these ions. Additionally, as can be seen in both Figures 5c and 6a, there is a small polarization of the charge density along the N−H···O hydrogen bonds.

A2. High-Pressure Behavior of AN IV. The compressibility of phase IV of AN has been investigated for the pressure range 0−600 GPa. These calculations have been performed in a two-step procedure. In the first step the optimizations have been done by maintaining the experimental *Pmmn* space group symmetry. In the second stage we have performed these optimizations in space group *P*1 to allow structural relaxations of all crystallographic parameters. These last calculations indicate no significant deviations from the orthorhombic symmetry imposed at the first step. The corresponding dependences of the lattice parameters and unit cell volume on pressure are represented in Figure 7.

In the low pressure regime (below 20 GPa) the compressibility is strongly anisotropic. In the directions of the *a* and *c* axes the structure is much stiffer than along the b direction. Fits of the data for this pressure region indicate a linear compressibility almost equal for the *a* and *c* axes of about 0.04 Å/GPa and of 0.09 Å/GPa for the *b* axis. This different behavior can be understood based on the type of bonding for this phase. As presented in the introductory section, AN IV presents strong N(1)−H(1)···O(1) hydrogen bonds in the *ac* plane and somewhat weaker H2···O1 bonds along the b direction. Consequently, it is expected that the compressibility properties of AN IV be similar for the *a* and *c* directions but different from the *b* directions which has the highest compressibility. In the region of higher pressures, above 60 GPa, the compressibilities along the three axes become almost equal. Indeed, as can be seen in Figure 7a the curves describing the variation of the lattice parameters with pressure are almost parallel for the high-pressure regime. This behavior can be understood as being due to an increase of the charge overlap and a change of the bonding character toward a covalent one. These changes determine equalization of the compressibilities for different axes.

From the pressure dependence of the unit cell volume in the range 0−150 GPa (see Figure 7b) we have determined the bulk modulus of AN IV based on a fit to the third-order Birch−Murnaghan equation of state[43]

$$p(V) = \frac{3}{2} b_0 \left[\left(\frac{V_0}{V}\right)^{7/3} - \left(\frac{V_0}{V}\right)^{5/3}\right]\left\{1 + \frac{3}{4}(b' - 4)\left[\left(\frac{V_0}{V}\right)^{2/3} - 1\right]\right\} \quad (8)$$

where V_0 is the unit-cell volume at zero pressure, b_0 is the bulk modulus and $b' = \partial b/\partial p$. The values obtained from the fit are

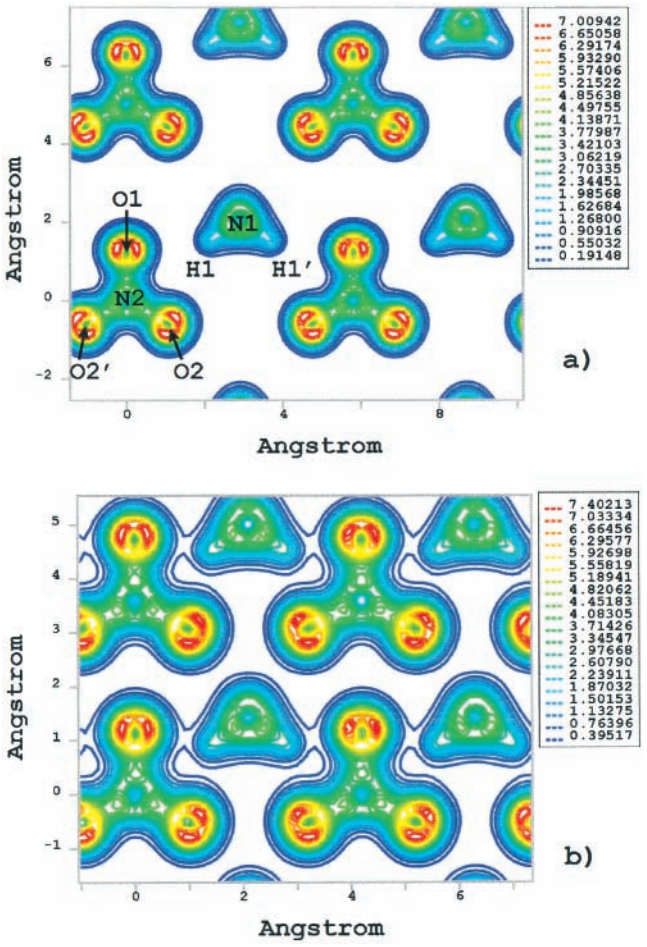

Figure 6. Contour plots of the valence electron density (units of electrons/Å^3) in the case of phase AN IV. The contours are taken along a plane perpendicular to [100] direction passing through the NH_4^+ and NO_3^- ions. Upper panel (a) corresponds to $P = 0$ GPa and lower panel (b) corresponds to $P = 400$ GPa.

$V_0 = 154.4$ Å^3, $b_0 = 23.6$ GPa and $b' = 5.0$. The calculated V_0 parameter is in very good agreement with experiment ($V_{0exp} = 153.99$ Å^3).

We have also investigated whether other crystallographic packings of the AN IV are possible in the high-pressure regime. In these cases we have started the optimizations using slightly tilted configuration states of the ammonium ions relative to the experimental configurations. These calculations have been done without any symmetry constraints (symmetry *P*1). We have found that for pressures above 75 GPa a slightly distorted monoclinic crystal symmetry is possible. We have identified the crystal symmetry in this case as belonging to the *P*21/*m* space group with a β angle of about 88.4°. The variation of the lattice dimensions and unit cell volume for this monoclinic structures are also presented in Figure 7a,b. As can be seen these variations of the lattice dimensions follow closely those determined for the orthorhombic symmetry while the volume of the unit cell is practically superimposable on that calculated for the *Pmmn* symmetry. These results indicate that it might be possible that the orthorhombic symmetry of AN IV changes to a monoclinic type at higher temperatures and pressures.

Additional insight in the effects of pressure on the electronic structure of AN IV has been obtained from calculations of the band structure and density of states. Selected results of these calculations are presented in Figures 8 and 9. From the analysis of these plots it appears that pressure has several major effects on the electronic structure of the crystal. First, there is a

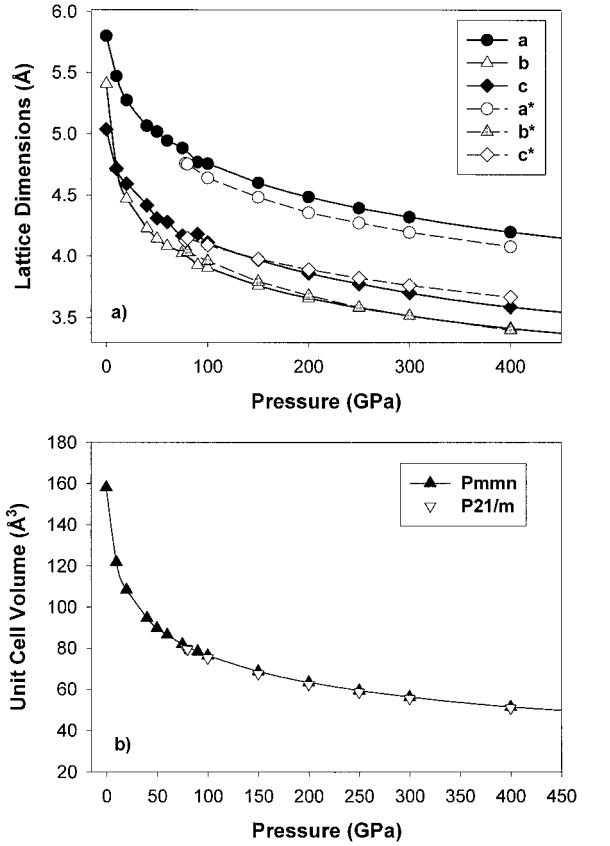

Figure 7. Variation of the lattice dimension and unit cell volume of AN IV crystal structure as a function of the hydrostatic applied pressure.

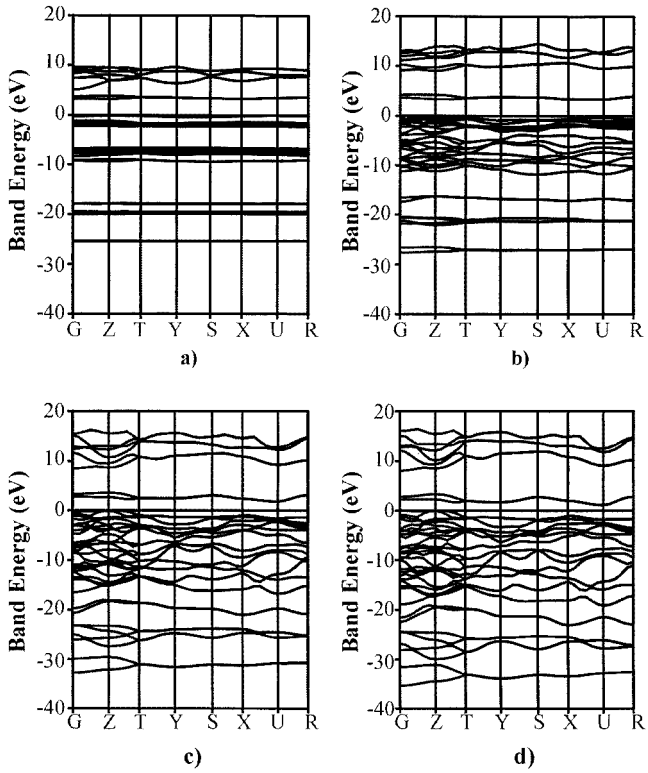

Figure 8. Band structure calculations for AN IV phase at pressures: (a) 0 GPa; (b) 100 GPa; (c) 400 GPa; (d) 600 GPa.

significant increase of the width of different groups of bands, an effect initially seen at the top of the valence bands (Figure 8b) and that extends at higher pressures toward the deeper bands (Figure 8c,d). This broadening of the bands leads to almost a

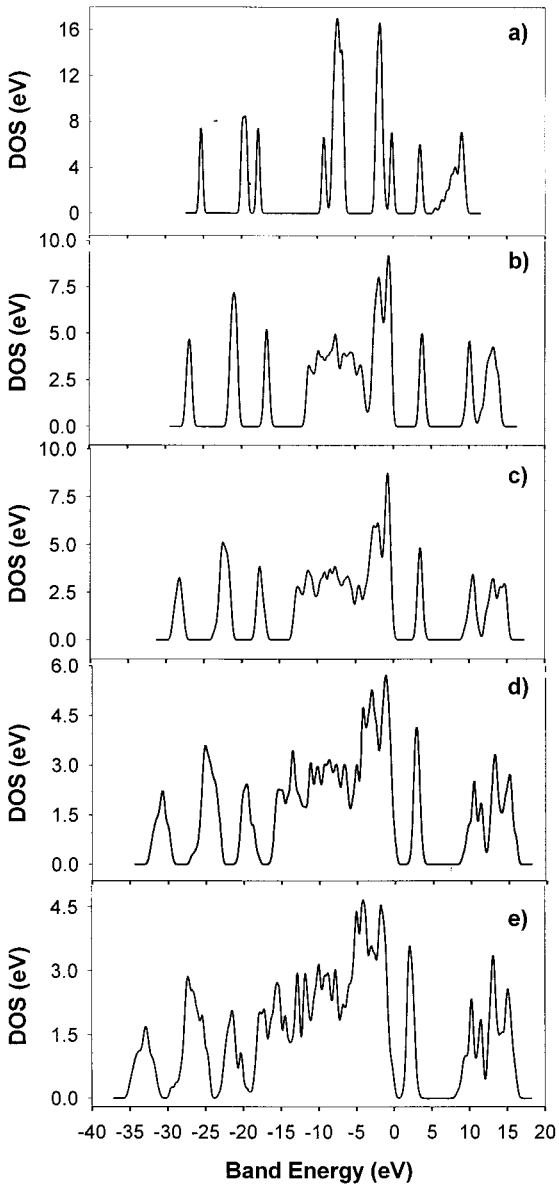

Figure 9. Calculated DOS for AN IV at pressures: (a) 0 GPa; (b) 100 GPa; (c) 200 GPa; (d) 400 GPa; (e) 600 GPa.

continuum of states for the highest pressure investigated (see Figure 9d,e). Additionally it can be seen that the bands are less and less flat across the Brillouin zone and they shift toward negative values with increasing pressure. These results also support the previous results related to the increase of charge overlap and to the change of the bonding character toward a covalent one. Because of the fact that in the highest pressure regime of 600 GPa (Figure 8d) the broadening of bands occurred for the deep valence bands the band structure results should be considered as qualitative. In this situation a more accurate description should go beyond the pseudopotential approximation and include all the electronic core levels.

Finally, the variation of the pressure causes a nonlinear change of the band gap (see Figure 10). In the pressures regime up to about 100 GPa the gap minimum increases slightly from 3.25 eV to about 3.37 eV. Over this pressure range the volume of the unit cell decreases by about 50%. Increasing of pressure beyond 100 GPa causes a sharp decrease of the band gap to 2.0 eV at 600 GPa. This rapid closure of the band gap indicates also a change in the conduction character of the crystal from an insulator toward a metallic system.

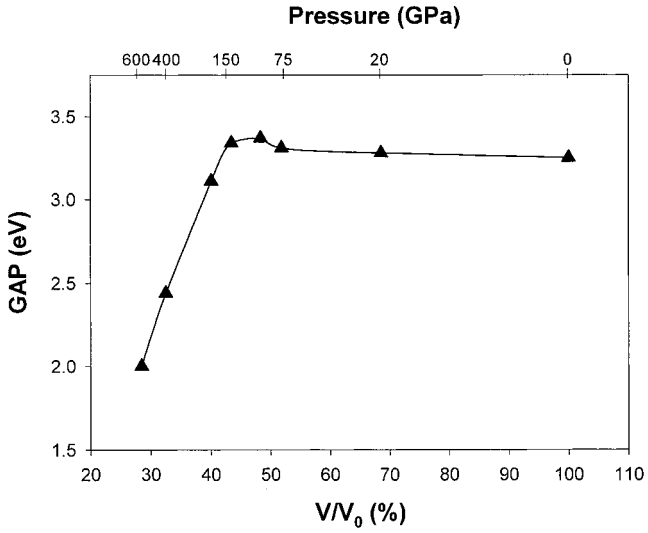

Figure 10. Variation of the band gap of AN IV crystal with pressure.

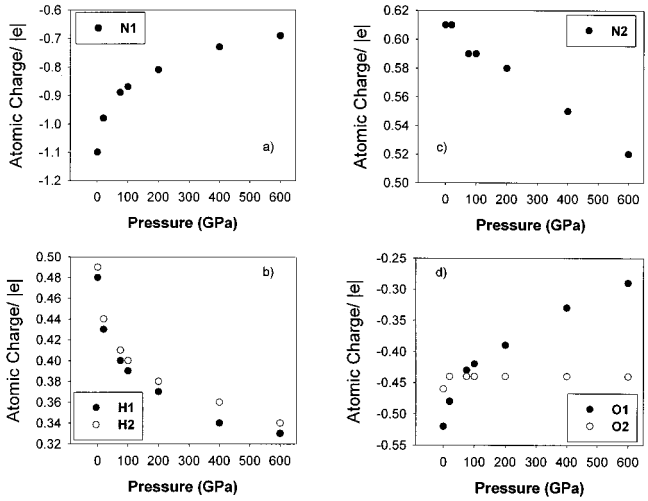

Figure 11. Variation of the Mulliken charges assigned to different atoms of NH_4^+ and NO_3^- ions as a function of pressure.

The effect of increasing pressure on the charge distribution can be seen in Figure 6b where a section through the charge density distribution parallel to the *aOc* crystallographic plane passing through the nitro and ammonium groups is given. These results are for 400 GPa. By comparing the distributions at $P =$ 0 and 400 GPa given in Figure 6a,b, one can see two effects. The first is related to the spread of charge around the individual ions leading to increased charge overlap. Second, there is a clear charge transfer and redistribution among the atoms.

An alternative way to describe the effect of charge rearrangement caused by compression of the lattice can be obtained by evaluation of the Mulliken charges of different atoms of the system. This has been achieved by the aid of the formalism developed by Segall et al.[44,45] Briefly this is done by projecting the eigenstates onto localized basis sets represented by the atomic pseudo-orbitals generated from the pseudopotentials used in the calculation. However, it is known that the Mulliken charges can provide only a qualitative description of the bonding characteristics. The variations of the individual atomic Mulliken charges as functions of pressure are shown in Figure 11, from which we observe that the variation of charges on the N atoms of the ammonium and nitrate ions inversely evoluates with increasing pressure, namely. it increases for ammonium nitrogen atoms and decreases for those in the nitrate ions. These changes take place together with a decrease in H atoms charges and a

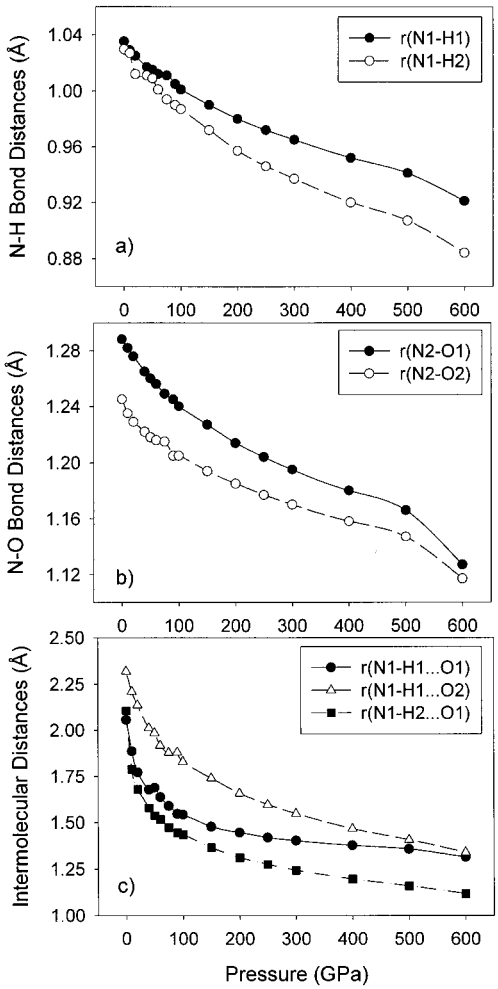

Figure 12. Pressure variation of selective intra- and intermolecular geometrical parameters of AN IV crystal.

significant increase of the charge on the O atoms of the nitro groups involved in hydrogen bonding (O1 atoms). The overall charges of the NH_4 and NO_3 ions decrease to values of 0.65e and −0.65e, respectively, at 600 GPa. The large charge redistributions seen as a result of lattice compression indicate a decrease of the ionic character of the crystal and a concomitant increase of the covalent character.

Finally we present in Figure 12 the modifications of the main intra- and intermolecular bond lengths with increasing pressure. Over the pressure range 0−600 GPa all intramolecular distances decrease continuously, specifically by 11−14% in the case of N−H bonds and by 10−12% for N−O bonds. As expected the intermolecular N−H···O distances undergoes even larger variations, between 36 and 47%. In the high-pressure regime, the O···H contacts are so close that practically new covalent O−H bonds are formed. These modifications are consistent with the changes in the charge distributions as well as with the decrease of the ionic character of the crystal.

B. Molecular Packing Calculations. The intra- and intermolecular potential parameters used to describe the physical properties of phase V of AN are presented in Table 3. The results of the molecular packing calculations obtained using the GULP program are given in Table 4. We have determined that the results are not dependent on whether the energy minimizations are done with or without symmetry constraints. Moreover, for the minimized configurations we have verified by phonon calculations that all the vibrational frequencies have positive values, indicating the existence of a local minimum.

The change in lattice and molecular parameters after energy minimization relative to the experimental structures are also given in parentheses in Table 4. The maximum deviations of the lattice dimensions are 2.4% for AN V with a deviation of only −1.15% for the unit cell volume. There is essentially no change in the values of the unit cell angles, which remain close to 90° consistent with the space group symmetry.

For the minimized configuration we indicate also in Table 4 the total lattice energy together with the corresponding electrostatic energy contribution. The electrostatic energy accounts for the largest part of lattice energy and thus the chosen set of electrostatic charges has the primary effect in reproducing the crystallographic parameters of the crystal. Additionally, in Table 4 we also give the calculated elastic constant for the optimized structure. No experimental data were available for comparison.

These results suggest that accurate descriptions of the equilibrium properties of the AN V crystal phase can be predicted by this potential.

C. NPT Molecular Dynamics Calculations. A more realistic prediction of the structural lattice parameters can be obtained by considering the molecular motion as a function of temperature and pressure instead of the one determined in molecular packing calculations, based on simple lattice energy minimization. For this purpose, we have determined the structural crystal parameters at atmospheric pressure and in the temperature range 4.2−255 K for phase AN V. These results are illustrated in Figure 13. At $T = 4.2$ K, the average lattice parameters for AN V are 8.0781, 7.8055, and 9.5948 Å, values which are practically identical with those predicted by molecular packing calculations. This is expected, since the thermal effects at 4.2 K should be minimal and the thermal averages at this temperature should be close to the values corresponding to the potential energy minimum. A similar good agreement is obtained when experimental data collected at 78 K[3] are compared to the predicted data at 100 K; these differ by 3.09%, 0.76%, and 2.00%, respectively, for lattice dimensions *a*, *b*, and *c*. Moreover for the entire temperature range investigated the unit cell angles remain approximately equal to 90°. From the dependence of the unit cell volume on temperature we can see the calculated results are practically superimposable on the experimental values in the temperature range 50−150 K. However, for the higher temperatures 200−250 K the predicted values start to shift slightly from the experimental data but still the deviations remain small. For example at $T = 250$ K, the relative error between the predicted ($V = 619.67$ Å^3) and the experimental ($V = 624.25$ Å^3) unit cell volume is only 0.73%.

We have determined the corresponding linear and volume expansion coefficients (see Table 5) from the temperature dependence of the lattice parameters. The calculated values indicate that expansion along *a* and *b* axes are similar and much greater than the expansion along the *c* axis is extremely small. These findings are in agreement with previous results obtained in neutron diffraction studies.[3] The large differences between the expansions along *a* and *b* axes relative to the *c* axis are due to the fact that thermal properties of this phase are determined primarily by the amplitudes of out-of-plane motions of the nitrate ions. As the planar nitrate ions are perpendicular on both the *a* and *b* axes it follows that in AN V the largest expansion rates occur along these axes.

In Figure 14 we compare the radial distribution functions (RDFs) for different pairs of sites at different temperatures. For example, in Figure 14a we show the RDF for the pair N1−N2, where N1 and N2 denote the N atoms of the ammonium, respectively, nitrate ions. From these plots it is evident that

TABLE 3: Force Field Parameters for Crystalline Phases V of AN

intramolecular potential parameters			intermolecular potential parameters			electrostatic charges	
parameter	k_η[a]	η^0_V	parameter	A_V[b]	B_V	atom	charge/|e|
N_1-H	3699.1769	1.028	N−N	1904534.60	1508.90	N_1	−0.774701
N_2-O	3480.9346	1.264	O−O	1970959.87	2739.50	$H_{i,\,i=1-4}$	0.443675
$H-N_1-H$	327.8218	109.63	N−O	3735452.02	3484.43	N_2	0.896259
$O-N_2-O$	1092.3241	120.00	H−H	2195.37	124.87	$O_{i,\,i=1,3}$	−0.632086
$O-N_2-O-O$	794.2765	0.00	N−H	100441.03	454.45		
			O···H*	1662.97	674.54		

[a] The indicated force constants (k_η) have units of kJ/(mol·Å) for bond lengths, kJ/(mol·rad^2) for bond angles, and kJ/mol for torsional angles. The corresponding equilibrium values have units of Å for bond lengths and degrees for bond angles and torsional angles. [b] A_V and B_V denote the Lennard-Jones potential parameters as described by eq 1 for phase V. The corresponding hydrogen potential parameters, eq 2, are indicated by an asterisk.

TABLE 4: Comparison of the Calculated and Experimental Lattice Parameters and Total Energies for Phase V of AN[a]

	lattice energy[b]		lattice parameters[c]						
	E_{total}	E_{elect}	V	a	b	c	α	β	γ
exp[d]			611.7240	7.8850	7.9202	9.7953	90.0	90.0	90.0
calc	−744.7	−741.0	604.7140	8.0734	7.8058	9.5953	90.0	90.0	90.0
			(−1.15)	(2.39)	(−1.44)	(2.04)	(0.0)	(0.0)	(0.0)
			Elastic Constants for AN V[e]						
1	5.19863		4.56774	3.46721	0.00000		0.00000		0.00000
2	4.56774		5.91507	3.51771	0.00000		0.00000		0.00000
3	3.46721		3.51771	9.21854	0.00000		0.00000		0.00000
4	0.00000		0.00000	0.00000	1.25645		0.00000		0.00000
5	0.00000		0.00000	0.00000	0.00000		0.67791		0.00000
6	0.00000		0.00000	0.00000	0.00000		0.00000		2.08417

[a] The values in parentheses represent the percentage difference between the calculated and the experimental values. The corresponding elastic constants predicted for this phase are also indicated. [b] Total (E_{total}) and electrostatic (E_{elec}) lattice energies are given in kJ/mol. [c] Lattice dimensions a, b, c are in angstroms and the angles α, β, and γ in degrees. [d] Experimental values from ref 3. [e] The corresponding units are 10 GPa.

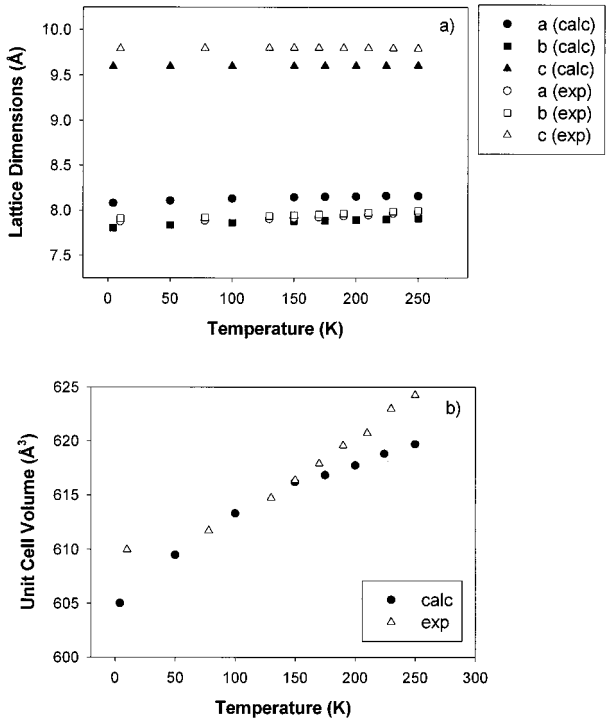

Figure 13. Lattice dimensions and unit cell volume variations for AN V as a function of temperature as determined in NPT-MD simulations.

increasing the temperature from 4.2 to 250 K does not produce any significant displacement of the ionic centers of mass. Indeed, the RDFs at these temperatures correspond to well ordered structures with correlation at long distances. The positions of the major peaks do not change significantly and the main temperature effect is the broadening of the peaks with partial overlapping of some of them. These results indicate that there is no translational disorder of this phase as a function of temperature.

TABLE 5: Linear and Cubic Expansion Coefficients for AN V Phase As Determined from Fits of the Form $\chi = \chi_0(1 + \chi_1(T - T_0) + \chi_2(T - T_0)^2 + \chi_3(T - T_0)^3)$

parameter[a]	a	b	c	V
χ_0	8.078	7.805	9.595	604.95
$10^5\chi_1$	8.51	10.40	0.57	19.42
$10^8\chi_2$	−22.22	−37.81	−2.51	61.34
$10^{11}\chi_3$	16.54	70.98	6.84	91.48
T_0	4.2	4.2	4.2	4.2

[a] The units are Å, K^{-1}, K^{-2} and K^{-3}, respectively. Å^3, K^{-1}, K^{-2} and K^{-3} for coefficients χ_0, χ_1, χ_2, χ_3 in the case of lattice lengths and unit cell volume, respectively.

Further insight into the crystallographic structure can be obtained by analyzing the site−site RDFs for the case of shorter contacts, i.e., the N−O···H intermolecular bonds. These RDFs were calculated as averages over all molecules in the MD box but limited by the cutoff distance used in potential calculation. The results are represented in Figure 14b−d for the temperatures of 4.2 and 250 K, respectively. The peaks in these distributions of the hydrogen bonds corresponding to short intermolecular distances (below 2.0 Å) are clearly evident. Moreover, with increasing temperature the positions of these peaks are practically unchanged and their individualities are maintained. These findings indicate the lack of rotational disorder of the ions with increasing temperature in agreement with the ordered character of phase V of AN.

IV. Summary and Conclusions

The results presented in this study show that reliable data about the electronic, geometric and dynamic properties of AN

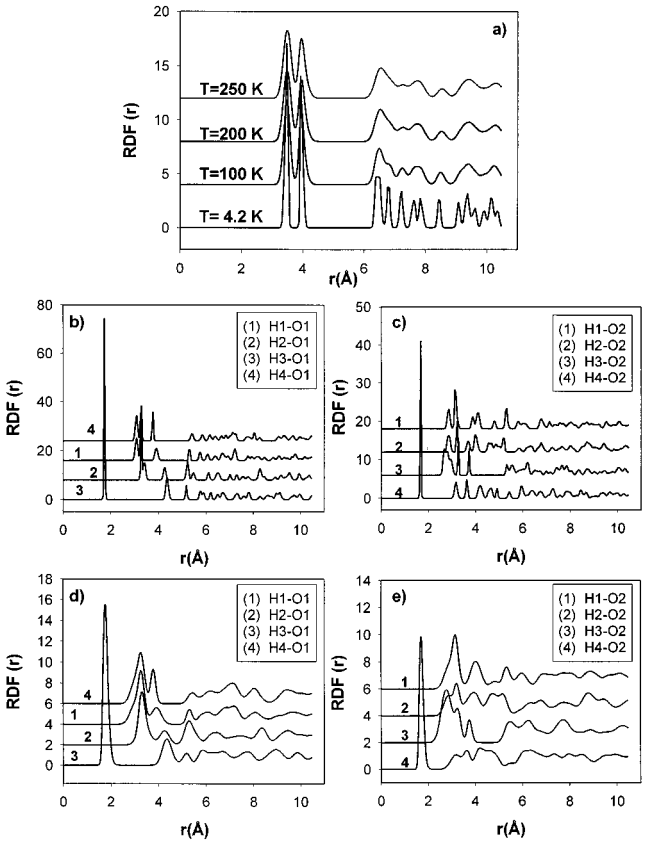

Figure 14. Radial distribution functions for the N1···N2 and selected N−O···H pairs as a function of temperature. N1 and N2 denote the N atoms of ammonium and respectively nitrate ions. (b) and (c) correspond to $T = 4.2$ K, and (d) and (e) to $T = 200$ K.

in its different phases can be obtained by combined use of plane-wave total energy calculations based on DFT theory and the pseudopotential method coupled with molecular dynamics calculations based on classical fitted potentials. The major findings of this work can be summarized as follows:

(1) The geometrical features of the AN in phases V and IV are well reproduced by our calculations and are in excellent agreement with the structural configurations determined experimentally by neutron diffraction technique.[3,7,9] An acceptable agreement was also obtained for phase II despite the existence of a disordered structure for this phase. The largest differences between the calculated and the experimental crystallographic parameters are for phase III where dynamical disordered motions and temperature effects have a strong influence on crystal structure. In this case the structure is not well represented by our static, zero temperature ab initio calculations.

(2) The results of band structure calculations and the analyses of the density of states indicate that AN in its different phases V, IV, III and II is an electrical insulators with, respectively, band gaps of 3.44, 3.18, 3.37, and 3.51 eV. The structure of the occupied bands is characterized by the lack of dispersion along the Brillouin zone. The separation distances between different groups of bands is as large as a few eV. The top of the valence band is given by contributions of O(2p) from the nitrate ions and N1(2p) levels from the ammonium ions.

(3) Under hydrostatic compression phase IV maintains orthorhombic symmetry up to high pressures but at high pressures and temperatures a phase with monoclinic might be also possible. In the low pressure regime the compression is highly anisotropic. This behavior is determined by the nature of hydrogen bonding in the crystal with strong infinite two-dimensional hydrogen bonds in the aOc plane and weaker van der Waals bonds along the *b* axis. In the high-pressure regime the compression becomes more isotropic due to the increase of charge overlap and change of the bonding character toward a covalent one. The calculated bulk modulus determined from the variation of the lattice volume with pressure based on Birch−Murnaghan equation of state is $b_0 = 23.6$ GPa.

Increasing the pressure has strong effects on the electronic properties of the crystal. Mainly there are large broadenings of the electronic occupied bands and shifts of them toward lower energies. Additionally we have found the in the pressure range 0−100 GPa there is a slight increase of the band gap from 3.25 to 3.37 eV followed by a sharp decrease to 2 eV at 600 GPa. The change of the electrical character from an insulator toward a metallic one takes place with strong charge redistributions over different atoms of the crystal and by large changes of the intra- and intermolecular geometrical parameters.

(4) We have developed an intra- and intermolecular potential to describe phase V of AN. This potential is based on further development of our previous intermolecular potential for the ammonium dinitramide crystal[22] and contains 6-12 Lennard Jones potentials, 10-12 hydrogen-bond terms plus Coulombic interactions. Electrostatic charges of the ammonium and nitrate ions were determined from fits to ab initio electrostatic potentials calculated at the MP2/6-31G** level. The values of the intermolecular potential parameters were optimized to minimize the difference between the theoretical and experimental[3] structures.

A prime test of the proposed potential was done in symmetry-unconstrained molecular packing calculations. It was shown that the predicted crystallographic parameters are in good agreement with experimental parameters with maximum differences of 2.4%. We present also the full matrix of elastic coefficients for the optimized structure.

(5) The temperature dependencies of the physical parameters for phase V have been investigated by performing isothermal−isobaric molecular dynamics simulations at zero pressure over the temperature range 4.2 to 250 K. The results of these calculations show that the model accurately reproduces the experimental unit cell dimensions with a maximum deviation of 3.4%. Additionally, there is little translational and rotational disorder of the ions in the crystal. We have found that the hydrogen-bonding peaks in RDFs remain practically unchanged even at the highest temperatures considered in these simulations.

The linear and volumic thermal expansion coefficients of the crystal were determined from the averages of lattice dimensions extracted from trajectory calculations. The results obtained indicate anisotropic behavior of the crystal with expansions preferentially along the a and b axes and very small expansion along the *b* axis.

This model is useful for predicting nonreactive processes in AN V crystal. Further developments of the model will consider description of the other phases of AN and the corresponding phase transitions between these phases.

Acknowledgment. This work was supported by the Air Force Office of Scientific Research. We gratefully acknowledge the computational resources provided by ASC MSRC supercomputer center.

References and Notes

(1) Oommen, C.; Jain, S. R. *J. Hazardous Mater*. **1999**, *67*, 253.
(2) Kondirkov, B. N.; Annikov, V. E.; Egorshev, V. Y.; DeLuca, L.; Bronzi, C. *J. Propulsion Power* **1999**, *15*, 763.
(3) Choi, C. S.; Prask, H. J. *Acta Crystallogr*. **1983**, *B39*, 414.

(4) Ahtee, M.; Smolander, K. J.; Lucas, B. W.; Hewat, A. W. *Acta Crystallogr*. **1983**, *C39*, 651.
(5) Lowry, T. M.; Hemmings, F. C. *J. Soc. Chem. Ind*. **1920**, *39*, 101.
(6) Hoden, J. R.; Dickinson, C. W. *J. Phys. Chem*. **1975**, *79*, 249.
(7) Choi, C. S.; Mapes, J. E.; Prince, E. *Acta Crystallogr*. **1972**, *B28*, 1357.
(8) Lucas, B. W.; Ahtee, M.; Hewat, A. W. *Acta Crystallogr*. **1979**, *B35*, 1038.
(9) Choi, C. S.; Prask, H. J.; Prince, E. *J. Appl. Crystallogr*. 1980, *13*, 403.
(10) Brown, R. N.; McLaren, A. C. *Proc. R. Soc. London* **1962**, *A266*, 329.
(11) Lucas, B. W.; Ahtee, M.; Hewat, A. W. *Acta Crystallogr*. **1980**, *B36*, 2005.
(12) Goodwin, T. H.; Whetsone, J. *J. Chem. Soc*. **1947**, 1455.
(13) Brown, R. N.; McLaren, A. C. *Proc. R. Soc. London* **1962**, *A266*, 329.
(14) Ahtee, M.; Kurki-Suonio, K.; Lucas, B. W.; Hewat, A. W. *Acta Crystallor*. **1979**, *A 35*, 591.
(15) Engle, W. *Explosivstoffe* **1973**, *1*, 9.
(16) Owens, F. J. *J. Appl. Phys*. **1982**, *53*, 368.
(17) Cady, H. H. *Prop. Explos*. **1981**, *6*, 49.
(18) Bardo, R. D. In *Shock Waves in Condensed Matter*; Gupta, Y. M., Ed.; Plenum Press: New York, 1985.
(19) Coffey, S. F. *Phys. Rev.* **1981**, *B 24*, 6984.
(20) Gilman, J. J. *Philos. Mag*. **1993**, *B 78*, 207.
(21) (a) Sorescu, D. C.; Rice, B. M.; Thompson, D. L. *J. Phys. Chem*. **1997**, *101*, 798. (b) Sorescu, D. C.; Rice, B. M.; Thompson, D. L. *J. Phys. Chem*. **1998**, *B102*, 948. (c) Sorescu, D. C.; Rice, B. M.; Thompson, D. L. *J. Phys. Chem*. **1998**, *B102*, 6692. (d) Sorescu, D. C.; Rice, B. M.; Thompson, D. L. *J. Phys. Chem*. **1998**, *A102*, 8386. (e) Sorescu, D. C.; Rice, B. M.; Thompson, D. L. *J. Phys. Chem*. **1999**, *A103*, 989.
(22) Sorescu, D. C.; Thompson, D. L. *J. Phys. Chem. B* **1999**, *103*, 6774.
(23) Sorescu, D. C.; Thompson, D. L. *J. Phys. Chem. B* **1997**, *101*, 3605.
(24) Payne, M. C.; Allan, D. C.; Arias, T. A.; Johannopoulus, J. D. *Rev. Mod. Phys*. **1992**, *64*, 1045.
(25) White, J. A.; Bird, D. M. *Phys. Rev*. **1994**, *B50*, 4954.
(26) Monkhorst, H. J.; Pack, J. D. *Phys. Rev*. **1976**, *B13*, 5188.
(27) Kleinman, L.; Bylander, D. M. *Phys. Rev. Lett*. **1980**, *45*, 566.
(28) Lin, J. S.; Qteish, A.; Payne, M. C.; Heine, V. *Phys. Rev*. **1993**, *B47*, 4174.
(29) Francis, G. P.; Payne, M. C. *J. Phys. Condens. Matter* **1990**, *2*, 4395.
(30) Pertsin, A. J.; Kitaigorodsky, A. I. *The Atom-Atom Potential Method, Applications to Organic Molecular Solids*; Springer-Verlag: Berlin, 1987.
(31) Gale, J. D. *Philos. Mag.* **1996**, *B 73*, 3.
(32) Gale, J. D. *J. Chem. Soc., Faraday Trans*. **1997**, *93*, 629.
(33) Ewald, P. P. *Ann. Phys*. **1921**, *64*, 253.
(34) Möller, C. M. S. *Phys. Rev*. **1934**, *46*, 618. Hehre, W. J.; Ditchfield, R.; Pople, J. A. *J. Chem. Phys*. **1972**, *56*, 2257. Hariharan, P. C.; Pople, J. A. *Theor. Chim. Acta* **1973**, *28*, 213. Gordon, M. S. *Chem. Phys. Lett*. **1980**, *76*, 163.
(35) Frisch, M. J.; Trucks, G. W.; Schlegel, H. B.; Scuseria, G. E.; Robb, M. A.; Cheeseman, J. R.; Zakrzewski, V. G.; Montgomery, J. A.; R. E. Stratmann, J. Burant, C.; Dapprich, S.; Millam, J. M.; Daniels, A. D.; Kudin, K. N.; Strain, M. C.; Farkas, O.; Tomasi, J.; Barone, V.; Cossi, M.; Cammi, R.; Mennucci, B.; Pomelli, C.; Adamo, C.; Clifford, S.; Ochterski, J.; Petersson, G. A.; Ayala, P. Y.; Cui, Q.; Morokuma, K.; Malick, D. K.; Rabuck, A. D.; Raghavachari, K.; Foresman, J. B.; Cioslowski, J.; Ortiz, J. V.; Baboul, A. G.; Stefanov, B. B.; Liu, G.; Liashenko, A.; Piskorz, P.; Komaromi, I.; Gomperts, R.; Martin, R. L.; Fox, D. J.; Keith, T.; Al-Laham, M. A.; Peng, C. Y.; Nanayakkara, A.; Gonzalez, C.; Challacombe, M.; Gill, P. M. W.; Johnson, B.; Chen, W.; Wong, M. W.; Andres, J. L.; Gonzalez, C.; Head-Gordon, M.; Replogle, E. S.; Pople, J. A. *Gaussian 98*, Revision A.7; Gaussian, Inc.: Pittsburgh, PA, 1998.
(36) Forseman, J. B.; Frisch, A. In *Exploring Chemistry with Electronic Structure Methods*; Gaussian Inc.: Pittsburgh, PA, 1996.
(37) See, for example, Wiberg, K. B.; Rablen, P. R. *J. Comput. Chem*. **1993**, *14*, 1504 and references herein.
(38) Breneman, C. M.; Wiberg, K. B. *J. Comput. Chem*. **1990**, *11*, 361.
(39) Melchionna, S.; Ciccotti, G.; Holian, B. L. *Mol. Phys.* **1993**, *78*, 533.
(40) DL_POLY is a package of molecular simulation routines written by W. Smith and T. R. Forester, copyright The Council for the Central Laboratory of the Research Councils, Daresbury Laboratory at Daresbury, Nr. Warrington, 1996.
(41) Allen, M. P.; Tindesley, D. J. *Computer Simulation of Liquids*; Oxford University Press: New York, 1989.
(42) Hamilton, W. C.; Ibers, J. A. *Hydrogen Bonding in Solids*; Benjamin: New York, 1968.
(43) Poirier, J. P. *Introduction to the Physics of the Earth's Interior*; Cambridge University Press: Cambridge, U.K., 1991.
(44) Segall, M. D.; Pickard, C. J.; Shah, R.; Payne, M. C. *Phys. Rev*. **1996**, *B54*, 16317,
(45) Segall, M. D.; Pickard, C. J.; Shah, R.; Payne, M. C. *Mol. Phys.* **1996**, *89*, 571.